applied sciences

MDPI

Article

Generation of Monodispersed Spherical Thermosensitive Gels and Their Swelling and Shrinking Behaviors in Aqueous Polymeric Solutions

Raden Rinova Sisworo [1,2], Masato Hasegawa [3,*], Kousuke Nakashima [1], Yu Norimatsu [1] and Yukio Tada [3]

[1] Graduate School of Natural Science and Technology, Kanazawa University, Kakumamachi, Kanazawa 920-1192, Japan; raden_rinova@stu.kanazawa-u.ac.jp (R.R.S.); kn1011au@gmail.com (K.N.); graceyuas@gmail.com (Y.N.)

[2] Ministry of Education & Culture of Indonesian Government (Kemdikbud R.I), Faculty of Engineering, Universitas Halu Oleo, Kota Kendari 93132, Sulawesi Tenggara, Indonesia

[3] Faculty of Mechanical Engineering, Institute of Science and Engineering, Kanazawa University, Kakumamachi, Kanazawa 920-1192, Japan; tada@se.kanazawa-u.ac.jp

* Correspondence: mhase@se.kanazawa-u.ac.jp

Received: 13 February 2020; Accepted: 10 March 2020; Published: 16 March 2020

Abstract: This study investigates the factors affecting the formation of monodispersed thermosensitive gels and the parameters influencing the movement of gel particles containing N-isopropyl acrylamide in an aqueous polymeric solution in an upper heating system. Monodispersed thermosensitive gels were generated, and their swelling and shrinking behaviors were observed. The results revealed that continuous-phase flow rate and kinematic viscosity were most influential on the size of the monodispersed thermosensitive gels, which exhibited swelling and shrinking at both low and high temperatures of the polymeric aqueous solution, respectively, and demonstrated negative thermal expansion. In a low-temperature solution, the buoyancy force acting on the gel particles exceeded the gravitational force, because of which the size of the gels increased and the gels to ascended. At higher temperatures, the gels shrank because the gravitational force outweighed the buoyancy force, causing the gels to descend. The gels with a larger diameter tended to have longer durations of vertical movements within the aqueous polymeric solution than the smaller-sized gels; moreover, equilibrium conditions were quickly achieved by the smaller gels.

Keywords: thermosensitive gels; polymeric aqueous solution; swelling and shrinking behavior; buoyancy force; gravitational force; mechanical movement

1. Introduction

Every material demonstrates a thermal response to temperature changes in its surroundings; therefore, a material's behavior could vary under different conditions. Most materials exhibit positive thermal expansion at high temperatures, although some materials may demonstrate negative thermal expansion. Thermosensitive gels are one such material; they shrink when submerged in high-temperature liquids such as aqueous polymeric solutions and then swell when submerged in cooler fluids. The thermosensitive gels used in this study were generated in a laboratory for application specifically in the upper heating system (or the lower cooling system) of a rectangular enclosure. Such systems have an disadvantageous property that limits heat transfer between two opposite horizontal walls; however, they offer an advantage: When thermosensitive gels and a polymeric solution fill the gap between the two opposite heat sources, the gels show distinctive mechanical behaviors of repetitive shrinking and swelling over a period of time. The system used in

this study comprises N-isopropyl acrylamide (NIPA) gels and sodium polyacrylate (PAANa) solution in an integrated system; these materials form the focus of this study's observations. Theoretically, an aqueous polymeric solution is considered as an aqueous fluid comprising water and polymeric substances at a certain concentration. Polymeric solutions are important because of their application in multiple pharmaceutical and biomedical contexts [1] such as drug delivery [2] and enzyme or protein modifications [3,4]. Currently, thermosensitive gels have attracted considerable attention because they can be created using physical or chemical cross-linkers and form a unique class of polymeric materials that can retain quantities of water while maintaining their own structures [5]. Thermosensitive gels may be in either a sol or a gel phase depending on their temperature. The sol phase is considered as a fluid state, whereas the gel phase is related to a rigid, non-fluid state in which the shape/physical structure is preserved. Typically, the sol–gel state can be achieved only via a thermal stimulus. For biomedical applications in particular, the condition is suitable for in situ hydrogel formation at close to human-body temperature without requiring additional chemical initiators [6]. Theoretically, depending on its thermal characteristics, a thermosensitive gel may have either a lower critical solution temperature (LCST) or an upper critical solution temperature [7,8]. NIPA gel swells in aqueous solutions and absorbs a certain amount of the solution at temperatures below its LCST. At temperatures above its LCST, the gel shrinks and discharges the absorbed solution. Moreover, significant changes in volume occur because of small temperature changes close to the gel's LCST [9–11]. Exposing NIPA gel to a monotonic load above its LCST reveals a tougher mechanical behavior than is evident below its LCST in terms of nominal stress, stretch, and Young's modulus. This makes the gel suitable for health applications such as the regeneration of damaged tissues [12]. Furthermore, when NIPA gels are submerged in an aqueous polymer solution in a rectangular cavity, they exhibit repetitive vertical motions for a certain length of time [13]. Hasegawa et al. used a polymeric solution (polyacrylamide [PAA]) as a fluid for surrounding the gels because its density is between those of the gels in their swollen and shrunken states. When the gels were heated in the upper layer, they began to shrink, their volume decreased, and their density increased above that of the surrounding fluid. Consequently, the gels slowly moved toward the bottom of the cavity. Similarly, when the gels were cooled in the cavity's lower layer, the gels started to swell, their volume increased, and their density became lower than that of the surrounding fluid; hence, the gels moved upward. These conditions enabled the gels to vertically move in cyclical motions. They used cylindrical-shaped thermosensitive gels that were flat on both sides. One of the gels showed a vertical motion frequency of one cycle per 10 min for a duration of 230 min within a PAA solution. Other gels became easily attached to each other; they frequently adhered to the walls of the rectangular cavity, which promptly stopped their vertical movements because of the large contact areas on their flat sides. However, observations of NIPA gel behavior within an upper heating rectangular cavity have not received considerable attention, and literature on this topic is quite limited. Oh et al. revealed that for NIPA gel particles that are smaller than 200 nm, as their cross-linking density decreases, the volume change of the NIPA particles becomes more discontinuous [14]. This result corresponds with that obtained by Tanaka and Li [15]. Furthermore, the behavior of the gels at lower temperatures of about 20 °C demonstrates that those gels with a lower cross-linking density tend to have higher swelling rates than those with higher cross-linking densities. In fact, the temperature at which the gels start to swell is higher for those gels with higher cross-linking densities [14]. Moreover, the swelling behavior of NIPA gels is enhanced by increasing the gels' porous structures [16–19]. The addition of an initiator, such as dodecyl dimethyl benzyl ammonium bromide (DDBAB) and ammonium persulfate (APS), produced a hydrophobic initiator, dodecyl dimethyl benzyl ammonium persulfate, which provides a heterogeneous initiation mechanism and triggers the development of macro-porous structures [18] and an increased temperature response in the gel, as reported by Zhao et al. [18,19]. Recently, NIPA gels of various shapes and sizes have been produced. To minimize size variations, monodispersed spherical-shaped gels are generally made in laboratory scales using microfluidic devices [20–25]. The droplet diameter is controlled by adjusting the droplet-breakup mechanism, which is affected by the capillary number of the continuous-phase

flow [26–28]. Previously, studies have reported that increases in flow-rate ratios and capillary numbers correspond to a significant decrease in droplet diameter [29,30]. The flow rate of the continuous phase plays a significant role in controlling droplet size. A reduced flow rate in the continuous phase affects the neck length, current contact angle, and mean drop-growth velocity, which in turn affects droplet formation [31]. Other studies highlight the significant effect of interfacial tension on droplet size [32,33]. Furthermore, density differences between the continuous-phase flow and the dispersed flow affect the formation of the droplet's diameter as has been explained by Scheele et al. [34]. Based on research by Leong et al., by implementing two different diameters of a capillary tube for a constant velocity of the dispersed-phase flow, the droplet-size formation in both tubes decreased as the continuous-phase flow velocity increased. In their study, the diameter difference between the capillaries was quite small; therefore, decreases in droplet size were primarily affected by the drag force triggered by the continuous-phase flow [35]. Similar to the results reported by Sugiura et al. [32] and Thorsen et al. [33], according to those reported by Umbanhowar et al., drop-size formation correlates with the interfacial tension in the two phases, in addition to capillary tip diameter and viscosity. Thus, during droplet formation, the detachment of a droplet from its capillary occurs when stream-wise forces exceed the force induced by interfacial tension [36]. Moreover, droplet size is affected by the junction geometry of the microfluidic devices, the flow rates of the continuous phase, and the physical characteristics of the fluid i.e., its interfacial tension and viscosity [37]. Furthermore, the effect of flat-tip wettability (metallic nozzle) on droplet-size formation revealed that when a droplet of liquid is applied to the wetted flat tip of the nozzle, further adhesion forces occur on the base of the droplet and affect the attachment range. Hence, the intensity of adhesion tensions in the metal phase, the dispersed phase, and the continuous phase determine the contact area of the phase fluids, which consequently affect the droplet size [38]. Schneider et al. reported a flow-focusing method in which the initial strength of polymer concentration affected the droplets' mean particle-size distribution [39]. A high polymeric concentration caused an increase in mean particle-size distribution, which was attributed to the correlation between lower concentrations of polymer solution and lower viscosity of the dispersed phase and vice versa. Therefore, the force required by the droplet to break off from its dispersed-phase flow reduced [39]. Studies have also suggested that a lower concentration of polymeric solution in the continuous-phase flow is preferable for narrower particle dispersion. Similar results were reported by Zhu et al. regarding the formation of microspheres using a modified water-in-oil-in-water emulsion solvent-evaporation technique [40]. The effects of orifice length and width on droplet size in a flow-focusing device were investigated by Gupta et al. [41]. Their research revealed that by increasing the orifice length, the droplet size exponentially decreased until it became constant at a certain critical length and continued further beyond this length. Furthermore, by increasing the width of the orifice, a non-linear increase in droplet size occurred, and a constant orifice width resulted in the creation of a smaller-sized droplet as the capillary number increased. In their study, the effect of the capillary number on droplet size was similar to the findings reported by Wu et al. [29] and Hong et al. [30]. Regarding the connection between continuous-phase velocity and drop-formation time, the higher the velocity of the continuous-phase flow, the lower the drop-formation time [20]. Other studies highlight the effect of the continuous-phase flow (bond number, capillary number, and viscosity ratio) on droplet-break-off length, droplet-break-off time, and droplet volume [25]. Increasing the continuous-phase flow rate increased the flow's Reynolds number [22,24]. According to Sandulache et al., in one case, neither the continuous-phase flow rate nor the diameter of the external tube affected the average drop-size diameter in a jetting regime in which droplet breakage occurred some distance from the tip of the nozzle [27]. The episodic motions continuously occur provided a relevant condition supporting the movements that can be maintained, i.e., the satisfactory concentration of the solution, the appropriate gel diameter, and a preserved temperature difference between the upper and lower walls of the enclosure. The cyclical motion of the gels within the cavity is a function of time and is determined by the sum of the external forces acting on the gels, including gravity, drag, and buoyancy. In particular, these forces are affected by variables such as solution density,

gel density, drag coefficient, and gel size. To summarize, based on the abovementioned studies and as a continuation of the previous research reported by Hasegawa et al. [13], the current study's preference is for a typical gel with a smaller contact surface (i.e., a sphere). Gels of various sizes are required to observe their behavior in an upper heating system of a rectangular cavity filled with aqueous solutions. The spherically shaped monodispersed gels were generated using a microfluidic device with a constant micro-sized nozzle (outside diameter = 300 μm) by varying the viscosity and flow rate of the continuous-phase flow. The effects of viscosity and flow-rate variations of the continuous-phase flow on gel size formation, and the volume change of the gels together with their vertically repetitive motions within the aqueous solutions were investigated.

2. Materials and Methods

The methodology of this research entailed a two-stage experiment. This involved generating mono-dispersed thermosensitive gels and an investigation of the swelling and shrinking behaviors of these gels within a rectangular cavity filled with a polymeric aqueous solution. Each of the sections is described as follows.

2.1. Method for Generating Mono-dispersed Thermosensitive Gels

In this study, NIPA gels were generated by the cross-linked polymerization of the monomer (NIPA) and N,N′-methylenebisacrylamide (BIS) as cross-linker (see Figure 1), with the aid of other three chemicals and water measured in a unit mass. The method for synthesizing the gels was similar to that described by Zhao et al. [18,19]. The chemicals included 150 mg of NIPA (Wako Chemicals, Tokyo, Japan), 5 mg of BIS (Nacalai Tesque Inc., Kyoto, Japan), 25 mg of DDBAB (Wako Chemicals) as an initiator, 10 μL of N,N,N′,N′-tetramethylethylenediamine (TEMED) (Wako Chemicals) as an accelerator, 6 mg of APS (Nacalai Tesque Inc.) as an initiator, and 1.6 g of deionized water. NIPA, BIS, DDBAB, and TEMED were dissolved in half of the deionized water (0.8 g) and loaded into the first 3-mL syringe (inner diameter = 10.1 mm). Similarly, APS was dissolved in the remaining half of the deionized water (0.8 g) and loaded into the second 3-mL syringe. Two different viscosities of silicone oil (50×10^{-6} m^2/s and 300×10^{-6} m^2/s, Shin-Etsu Chemical, Tokyo, Japan) were used as continuous-phase fluids. Figure 2 shows the setup of the research apparatus. Based on the figures, the steps to synthesize the gels are described as follows: a 3 mL syringe containing NIPA components and another 3 mL syringe containing APS components were precisely mounted in the linear actuator module. The tips of both syringes were closely connected to the 2 mm square duct using the silicone tube, and the speed of both piston syringes was set to 0.002 mm/s. A video-recording camera was positioned close to the surface of the square duct to capture footage of the flowing gel droplets for subsequent analysis of their diameters. After inspecting all the connections, the linear actuator was activated. The actuator started pushing both piston syringes to deliver the NIPA and APS solutions at the same volumetric flow rate. Consequently, both solutions were deposited in front of the needle nozzle prior to mixing and before forming a gel solution (considered as dispersed flow). A constant dispersed flow rate (Q_d) of 3.2×10^{-10} m^3/s was maintained throughout the study. The gel solution was then ejected from the nozzle's tip (outside diameter = 300 μm) while the other co-flow of silicone oil (continuous-phase flow) was simultaneously ejected in the same direction by another pump (mzr-2521, HNP Mikrosysteme, Schwerin, Germany). The co-flows inside the square duct were primarily responsible for forming the gel droplets. Finally, all the gels were collected in a silicone oil reservoir on a cold plate, which was maintained at a constant temperature of −30 °C. In particular, the silicone tube within the reservoir was sufficiently long to increase the residence time of the gel droplets for the freezing process, which prevented droplet coalescence. The resulting gels were then stored in a freezer for 1 day to complete the polymerization process, and the diameter of the gel droplets flowing within the square duct was measured via image analysis. Based on the output of the diameter readings, the average diameter of the gels was calculated.

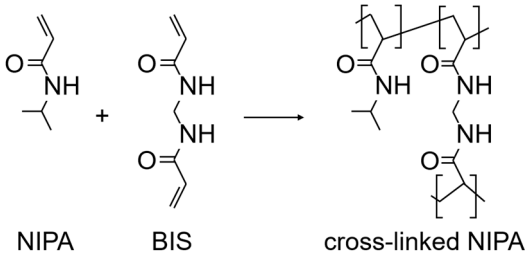

Figure 1. Synthesis of cross-linked N-isopropyl acrylamide (NIPA) gel.

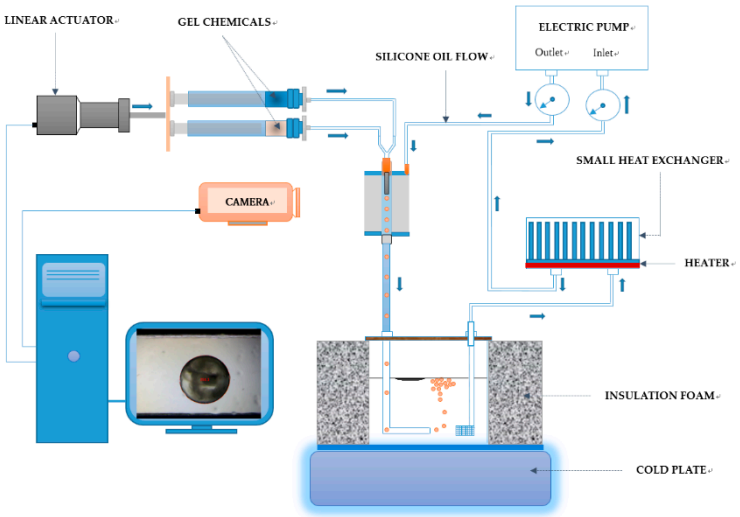

Figure 2. Schematic of the apparatus for generating the thermosensitive gels.

2.2. Method to Observe Swelling and Shrinking Behavior of the Gels

In this study, the behaviors of four typical-diameter thermosensitive gels (approximately 1.3 to 0.5 mm in water at 25 °C referred to as cases A, B, C, and D, respectively) were observed in two ways. The diameter of the gels varied because of different flow rates and viscosities of the continuous-phase flows used in the formation of the droplets. First, for each case, three gel particles were selected as samples and were submerged either in deionized water or in an 11 wt % aqueous solution of sodium polyacrylate (PAANa). The concentration of the PAANa solution was fixed throughout the experiment at 11 wt % to ensure a mass density in between those of the swelling and shrinking states of the gels; this enabled the gel particles to float at 10 °C and to sink at 40 °C. The PAANa powder (average molecular weight = ~2100, Sigma-Aldrich, St. Louis, Mo, USA) and the deionized water were mixed and stirred for about 15 min to ensure a diluted solution. During this observation, the temperature of each solution was adjusted from 5 to 40 °C in increments of 5 °C. Initially, the three gels were submerged in water, which was set to 5 °C. This condition was then maintained for 10 min before the size of the gels was recorded. Then, the water temperature was increased to 10 °C and again, after 10 min, the size of the gels was recorded. The same procedure was applied to determine the water temperature in 5 °C increments between 5 and 40 °C. After all the procedures were completed, the fluid was changed to an 11 wt % solution of PAANa. The data for this polymer solution were obtained in the same manner as that for water temperature. The recorded images were then analyzed to calculate the diameter of the three gels at different temperatures. Second, the vertical movements of the gels within the 11 wt % polymeric solution of PAANa were observed. Figure 3 shows the experimental apparatus for the observation. The primary parts of the apparatus comprised heating and cooling plates and a rectangular transparent acrylic cavity. The inner dimensions of the cavity were 16 × 16 mm (horizontal area) with a height of 13 mm. Initially, the temperatures of the hot wall (above in Figure 3) and the cold wall (below in Figure 3) of the cavity were maintained at 40 and 10 °C, respectively, using

water from thermostatic baths to create an upper heating system within the cavity. Eight gel particles were then inserted into the rectangular cavity, and images of their movements were captured every 20 s. Half (four out of eight) of the gels that exhibited active movements were then tracked in the post-processing stage.

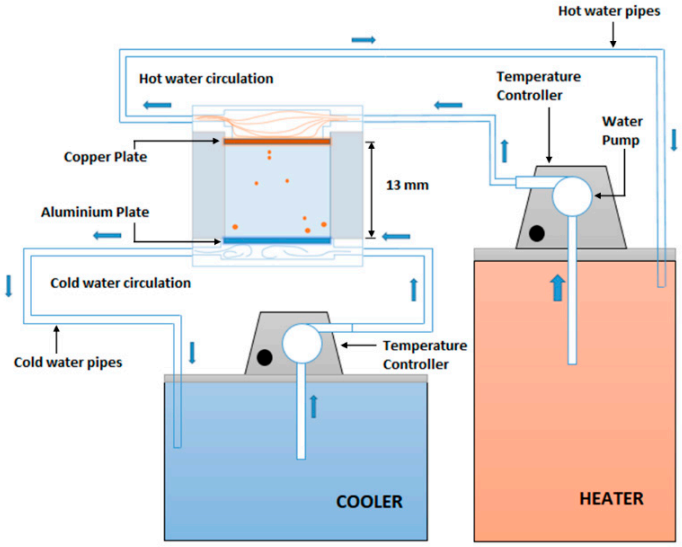

Figure 3. Schematic of the apparatus for mechanical observations.

3. Results and Discussion

The initial gel formation near the tip of the needle can be seen in Figure 4a–c, which shows the droplet's growth stage, its initial necking stage, and its final separation stage. All the monodispersed thermosensitive gels used in this study were generated in the microfluidic device by setting various flow rates for the silicone oil (50×10^{-6} m^2/s and 300×10^{-6} m^2/s) within a range of $3.96–15.8 \times 10^{-9}$ m^3/s. The growth stage of the droplet was defined as the point at which the new gel solution was ejected from the tip of the nozzle.

(**a**) (**b**) (**c**)

Figure 4. Images showing a droplet's formation at: (**a**) growth stage; (**b**) necking stage; (**c**) immediately after separation.

Simultaneously, the continuous-phase flow (silicone oil) with a constant flow rate generated drag in a vertical direction (in line with gravity), which, in this case, tended to separate the developing droplet from its gel solution on the tip of the nozzle. Droplet separation could either exist in a dripping regime or in a jetting regime. In the dripping regime, droplet breakage occurred at the tip of the nozzle (capillary tube). Meanwhile, in the jetting regime, droplet separation existed at the tip of a jet located far from the nozzle tip. In this research, droplet formation occurred in the dripping regime rather than in the jetting regime as the velocity of the inner fluid (dispersed phase) was much slower than that of

the continuous-phase fluid [27]. Hence, the condition supported the breakage of droplets (separation), which occurred near the tip of the nozzle, as shown in Figure 4. When the continuous-phase flow rate was gradually increased from 5.94×10^{-9} m^3/s to 15.8×10^{-9} m^3/s (for the both values of viscosity), the diameter of the gel droplets visibly decreased (as shown in Figure 5a with the reference letters A–D). The relationship between an increasing continuous-phase flow rate and the average droplet diameters for the both viscosities (50×10^{-6} m^2/s and 300×10^{-6} m^2/s) are shown in Table 1.

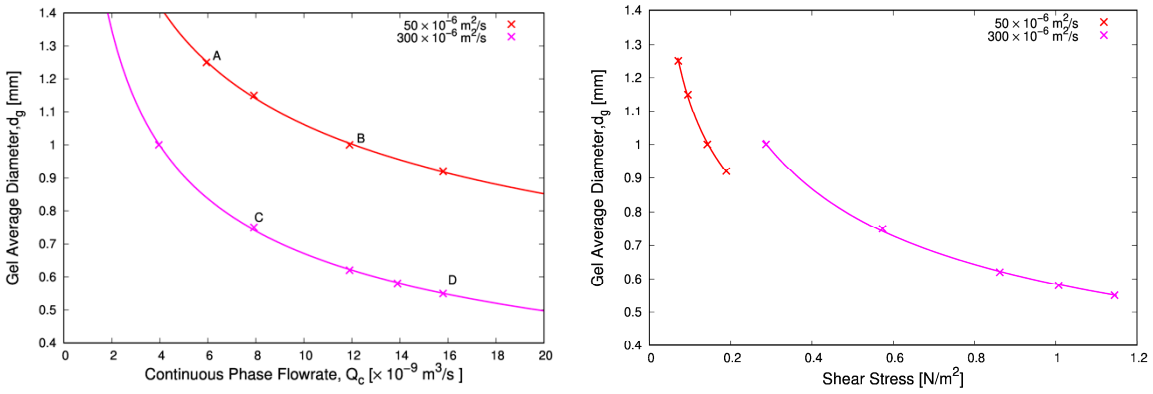

(**a**) (**b**)

Figure 5. Relationship between (**a**) the continuous-phase flow rate and the gel-droplets' average diameter and (**b**) the shear stress and the average diameter with respect to silicone oil viscosity.

Table 1. Average gel-droplet diameter for the two types of continuous-phase flows.

Flow Rate of 50×10^{-6} m^2/s ($\times 10^{-9}$ m^3/s)	Gel Diameter (mm)	Flow Rate of 300×10^{-6} m^2/s ($\times 10^{-9}$ m^3/s)	Gel Diameter (mm)
5.94	1.29	3.96	1.04
7.92	1.19	7.92	0.77
11.9	1.04	11.9	0.65
15.8	0.95	13.9	0.60
		15.8	0.57

A correlation was evident between the diameter of the generated droplet (d_g) and the flow rate of the continuous-phase flow (Q_c) for each of the silicone oils' viscosities, which can be expressed as follows:

$$d_g = 2.2{Q_c}^{-0.32} \text{ for } 50 \times 10^{-6} \text{ m}^2\text{/s silicone oil,} \quad (1)$$

and

$$d_g = 1.8{Q_c}^{-0.43} \text{ for } 300 \times 10^{-6} \text{ m}^2\text{/s silicone oil.} \quad (2)$$

The correlations indicate that the flow rate of the continuous phase significantly affected the diameter of the generated droplets.

The two curved lines shown in Figure 5a define the correlation between the continuous-phase flow rate and the average diameter of the droplets with respect to the two kinematic viscosity values of 50×10^{-6} m^2/s and 300×10^{-6} m^2/s. During the experiment, gel particles were prepared in nine cases by varying the continuous-phase flow rate and the kinematic viscosity. The coefficient of variations, the ratio of standard deviation, and the average value of the droplets' diameter calculated from hundreds of droplets for all the nine cases were <10%; therefore, droplet formation was considered to be monodispersed [25]. From the graph, it is apparent that the diameter of the droplets decreased as the continuous-phase flow rate increased; the same trend was evident for both kinematic viscosity values. In particular, the 50×10^{-6} m^2/s silicone oil could generate larger gel diameters than the 300×10^{-6} m^2/s silicone oil at the same continuous-phase flow rate values. A key result of these results

is that a higher-viscosity continuous-phase flow (300×10^{-6} m^2/s) can generate smaller gel droplets than a lower viscosity flow (50×10^{-6} m^2/s) or, more generally, the smaller the kinematic viscosity of the continuous-phase flow rate, the bigger the droplet diameter that can be generated. Moreover, this result was supported by the results of other researchers [24,38,42–44]. To illustrate this using one of the nine cases as an example, 7.92×10^{-9} m^3/s of the 50×10^{-6} m^2/s silicone oil generated a gel droplet of 1.19 mm in diameter. However, for the 300×10^{-6} m^2/s silicone oil with an identical flow rate, the diameter of the gel droplet was only 0.77 mm, i.e., the gel droplet decreased in volume by 72%. This significant decrease in the droplet's volume was clearly affected by an increasing flow rate and the kinematic viscosity of the continuous-phase flow. The increase in the continuous-phase flow rate correlated with an increase in drag induced by the flow, which supported droplet detachment from the tip of the nozzle. Hence, a smaller size of droplet was generated as the droplet-formation time was decreased. Furthermore, an increase in viscosity of the continuous-phase flow contributed to an increase in drag. According to Scheele et al., a greater drag force correlated with the diameter of the detached droplet [34]. Therefore, this study determined that droplet size was mostly affected by flow rate and the kinematic viscosity of the continuous-phase fluid (silicone oil). To examine the effect of these two factors on the droplet size, we estimated the shear stress on the interface as $\mu u_c/\delta$ where the average velocity u_c was continuous phased flow rate Q_c divided by the duct cross section (4 mm^2), neglecting the needle cross section which was less than 2 % of the duct's one. The reference length δ was taken as half the duct width. The dynamic viscosity μ was calculated using the densities of 958 and 966 kg/m^3 for 50×10^{-6} and 300×10^{-6} m^2/s silicone oils, respectively. The results are shown in Figure 5b. The two curves show a unified trend through the whole range of the shear stress, although there exists a discontinuity between them. It is presumably due to the difficulty to accurately evaluate the shear rate since the flow pattern was not simple around the droplet evolving near the nozzle tip in a narrow duct which width was comparable to the droplet size. Figure 6 shows images of the selected gels submerged in water at temperatures of 10, 25, and 40 °C for cases A and C and shows their physical appearance after polymerization. Three gel samples were selected and placed on an acrylic plate for observation. A similar shrinkage trend was exhibited by a cylindrical NIPA gel reported by Hasegawa et al. [13]. The size of the gel rod significantly decreased when the temperature of the solution was increased from 10 to 40 °C. At 40 °C, the NIPA gel shrank and demonstrated a negative thermal expansion characteristic.

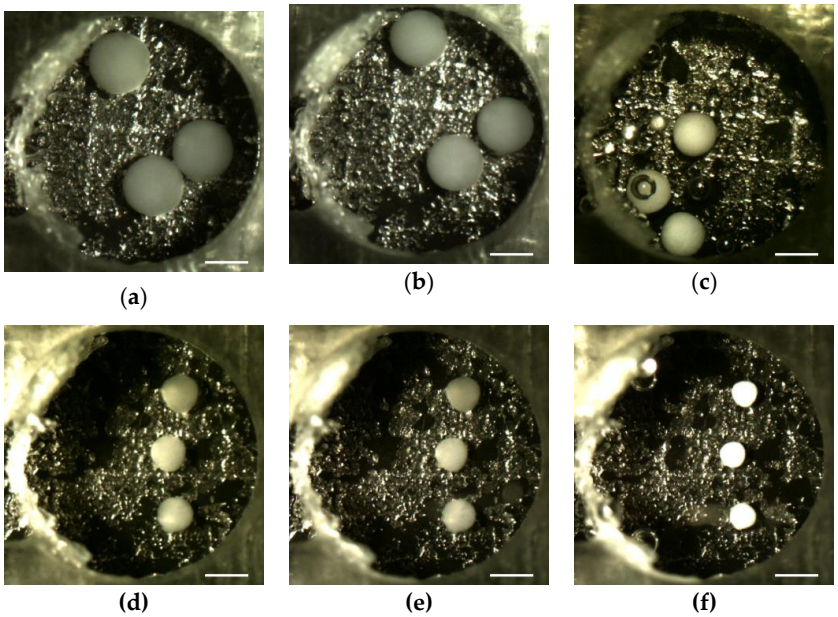

Figure 6. Gel particles submerged in water at elevated temperatures: (**a**) 10 °C; (**b**) 25 °C; (**c**) 40 °C in case A and (**d**) 10 °C; (**e**) 25 °C; (**f**) 40 °C in case C. The scale bar corresponds to 1 mm.

Figure 7 shows the variation in gel diameter for cases A, B, C, and D in water at different temperatures. Figure 8 shows the variations in gel diameter with the PAANa solution for the same-sized gels. Both figures show that as the temperature of the aqueous solution increased, the diameter of the gels oppositely decreased. This general correlation is evident for both solution types (water and the PAANa solution). Indeed, the exact pattern of both figures was different, especially within the range of 25–35 °C, where the most significant volume change occurred. For case A in both figures, considerable changes in gel diameter occurred at temperatures between 25 and 35 °C. For the smaller-sized gels, as shown in cases C and D, it is clear that the gels' average diameters slightly decreased as the water temperature increased. Moreover, cases A and B (which represent a bigger gel size) showed a significant decrease in diameter at temperatures between 25 and 35 °C as the temperature of the polymer solution increased. The vertical error bars shown in the plotted curves of the figures indicate a range of the three measured values.

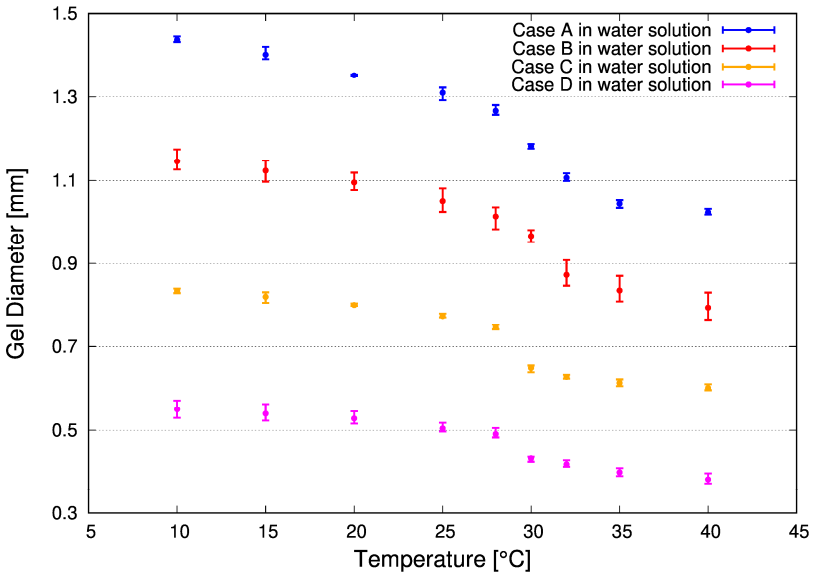

Figure 7. Variations in gel diameter at elevated temperatures in the water solution.

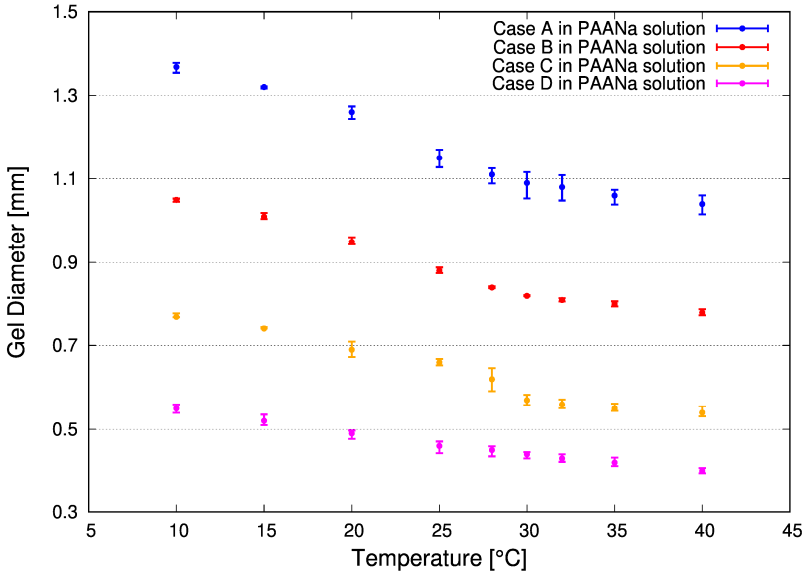

Figure 8. Variations in gel diameter at elevated temperatures in the sodium polyacrylate (PAANa) solution.

The plots reveal a slight decrease in gel diameter within two temperature ranges of the polymeric solution: 10–25 °C and 35–40 °C. However, in the temperature range between 25 and 35 °C, a sharp decrease in gel size is evident because significant changes in gel volume occurred within this range.

As shown in both graphs, a significant difference in the slope of the curve is observed at a temperature range between 25 and 30 °C. In this range, the gels exhibited a sharper response to the increasing temperature than the other two ranges. In particular, the largest slope is evident at temperatures between 25 and 30 °C. This phenomenon is attributed to the particular characteristics of the NIPA gel used in the experiment. At lower temperatures, the gels were in a swollen state and were larger in size. However, at higher temperatures, the gels shrank and became smaller as water molecules detached from the polymer chain (hydrophobic state). Water-molecule detachment started on the outer layer of the gels and continued to the inner layers. The plotted points represent the average value of the three gel samples, and the curve was obtained by polynomial (quaternary) approximation. The error bars in the figure represent the deviation in measured value at each temperature. The graph reveals that the diameter of the gel particles gradually decreased as the temperature of the polymer solution increased, indicating a negative expansion characteristic. When the temperature of the solution was constantly modified at specific intervals, the gels showed reversible transformation from a swelling state to a shrinking state before reverting to their initial state. Furthermore, the polymeric gel's higher molecular weight had a longer chain length and possessed a network with a lower cross-link density, which resulted in higher swelling rates in the gel [42].

The volumetric change in the gel particles is discussed below. A gel particle was approximated to a sphere of diameter d_g such that its volume V_g was estimated as $\pi {d_g}^3/6$. The relationship between V_g and the temperature of the gels in the aqueous solution T together with the relationship between the gels' volume ratio V_g/V_{shrink} and T can be seen in Figure 9, where V_{shrink} is the volume at 40 °C. The figures clearly demonstrate that case A, which is represented by the blue line, had the biggest gel volume, followed by cases B, C, and D. Figure 9b shows that the biggest change in gel volume occurred between 25 and 30 °C. In Figure 9a, the smallest gel (case D) showed no significant volume changes in the same range of temperature. Thus, by considering the volume ratio of gel V_g/V_{shrink}, the temperatures at which significant volume changes occurred could be clearly observed. Interestingly, as shown in Figure 9b, all sizes of gel exhibited similar volume ratio patterns when the temperature of the aqueous solution increased. However, the variation in ratios occurred in quite a small range between 2.7 and 3.0 at 10 °C. Moreover, a significant volume change occurred between 25 and 35 °C. It is evident from both figures that the largest volume change probably occurred at about 30 °C. Figure 10 shows the correlation between gel volume or the volume ratio and the temperature of the PAANa solution. For the PAANa solution, similar patterns of V_g–T were evident, as shown in Figure 10a. As the temperature of the PAANa solution increased from 10 to 40 °C, the volume of the gels in all cases inversely decreased. Figure 10b shows the relationship between the volume ratio and the temperature of the PAANa solution. The swelling volumes in the solution were lesser compared with those in water, while the volumes in a shrunken state at 40 °C were almost same as those in water, resulting in V_g/V_{shrink} values between 2.3 and 2.9. Note that the volume ratio of gels in the PAANa solution slowly decreased for the entire range as the temperature of the solution increased. This is in contrast to water for which the volume ratio significantly decreased between 25 and 35 °C, and the ratios remained almost constant at temperatures above this range. These differences in the two fluids are clearly illustrated in Figure 11, where only cases A and D were selected as examples.

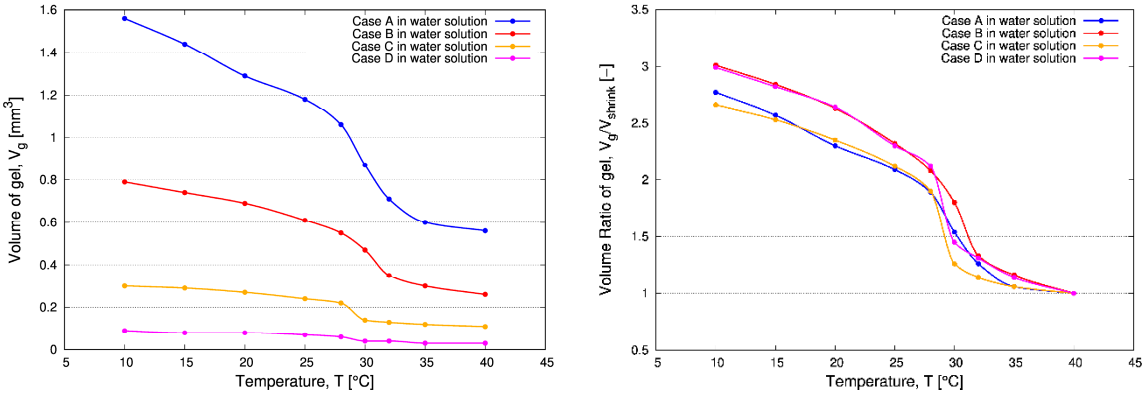

(**a**) (**b**)

Figure 9. Variations in (**a**) gel volume and (**b**) gel volume ratio at elevated temperatures in water.

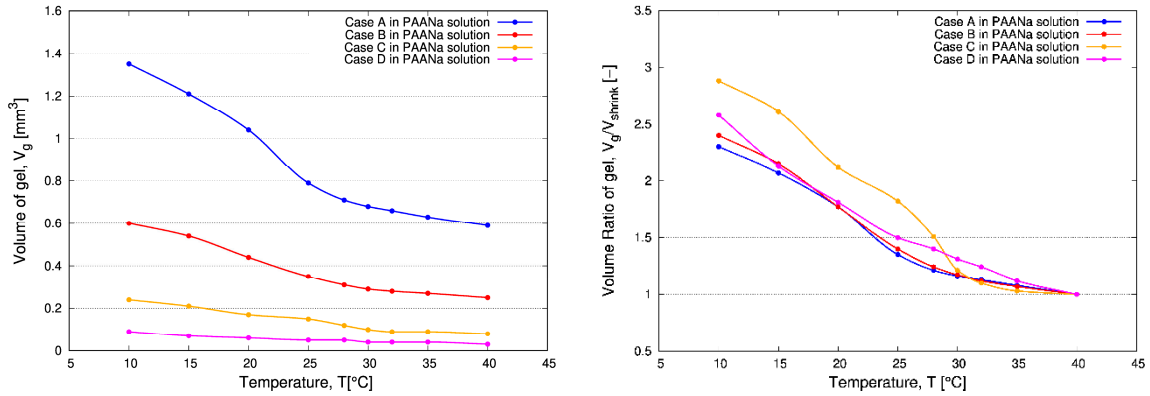

(**a**) (**b**)

Figure 10. Variations in (**a**) gel volume and (**b**) gel volume ratio at elevated temperatures in the PAANa solution.

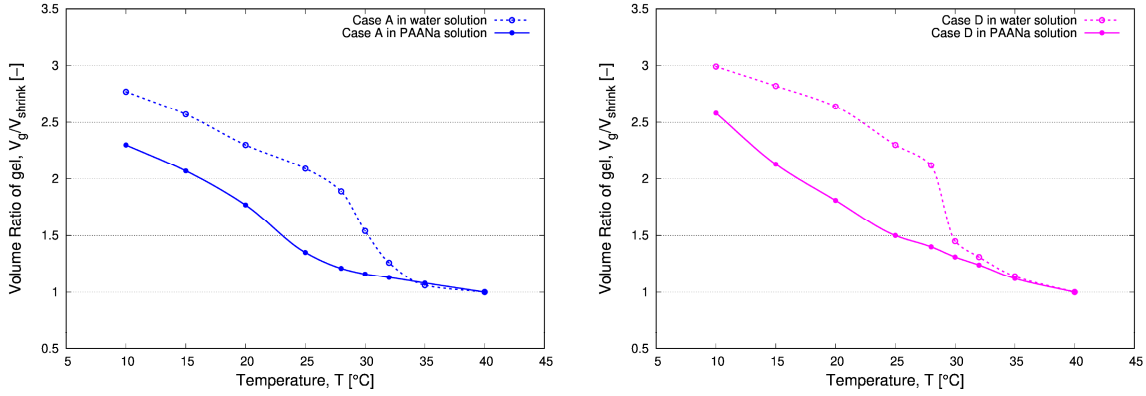

(**a**) (**b**)

Figure 11. Comparison of the volume ratio of gels in water and in the PAANa solution for (**a**) case A and (**b**) case D.

Figure 12 shows the periodic movements of the gels within the rectangular cavity. Eight gels were used in the experiment, and four active gels were selected for path tracking. The four gels can be identified by different colors (green, blue, red, and violet), which correspond to the curves in the following charts. The figures run in sequence from the top left image, where all the gels were still

at the bottom of the rectangular cavity, to the images on the right. Similar sequences were applied to the images in the second, third, and fourth rows. The gels were seen to be moving in vertical up-and-down cyclical patterns. Figure 13 shows the repetitive up-and-down movements of the gels within the PAANa solution for case A. The figure confirms that the gels moved vertically several times for a period of approximately 10 min before gradually damped in respect of time. The gels' movements were affected by the forces of buoyancy, drag, and gravity, which acted on the gels in the solution. At the start of the experiment, the swollen state gels were inserted into the polymer solution at 2 mm from the bottom of the cavity. The gels moved upward (because their density was lower than that of the polymer solution) until they reached a higher position 12 mm from the bottom of the cavity. In this position, the gels absorbed heat from the cavity's upper wall and transitioned to a state of shrinkage. Under this condition, the gels' densities increased above that of the polymer solution before moving downward for the first time until they were 1 mm from the bottom of the cavity. The lower temperature at the bottom caused the gels to transition to a swollen state. Moreover, buoyancy was higher in this position, which forced the gels upward until they reached the second-top position at 12 mm from the bottom of the cavity.

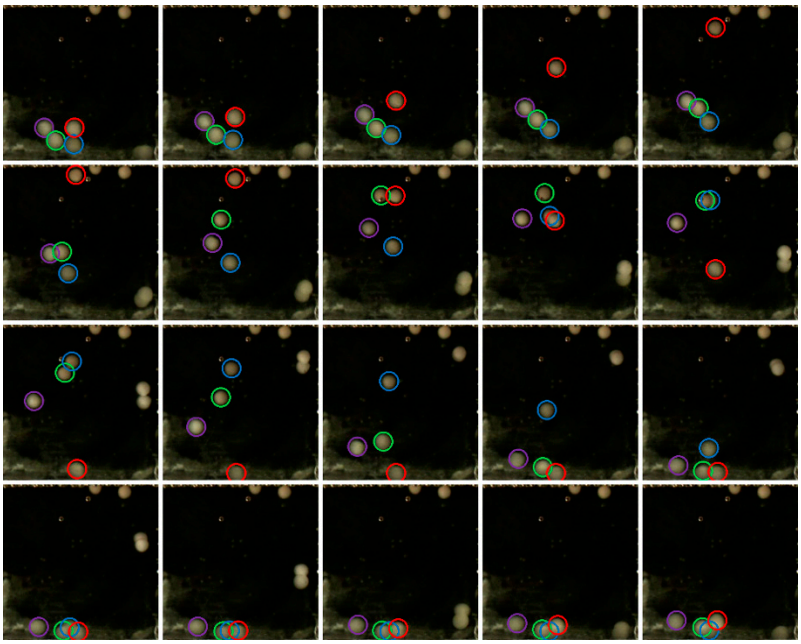

Figure 12. The periodic movement of gels (Case A) in the PAANa solution from 28–40.67 min after the start in increments of 40 sec. The trajectories of the particles in circles are shown in Figure 13 with the corresponding colors.

The top position of the gels gradually decreased over time. Two of the gels reached their equilibrium conditions earlier than the third gel; they then stopped moving between 4 and 4.5 mm from the bottom of the cavity. Evidently, at 170 min, the amplitude of gel 1 was considerably reduced because of collision and adhesion with gel 3, which caused a counteraction of their movements. The gels eventually broke up, and gel 1 started moving again; however, all the gels stopped moving at 250 min. Figure 14 shows the gel movements of case B. Although the amplitude of the vertical motion was small compared with case A, the gels exhibited similar movements for a period of 10 min followed by a gradual decrease in amplitude. At the start of the experiment for case B, some gels became stuck to the heat transfer surfaces (gels 1 and 4 were on top, and gel 3 was on the bottom). Gels 1 and 2 became affixed to other gels (whose trajectories are not shown) at 100 and 120 min, respectively, and could no longer be tracked. At 140 min, gel 4 became stuck to six other gels to form a cluster of seven. Gel 3 was the only gel that individually moved until the end of the experiment.

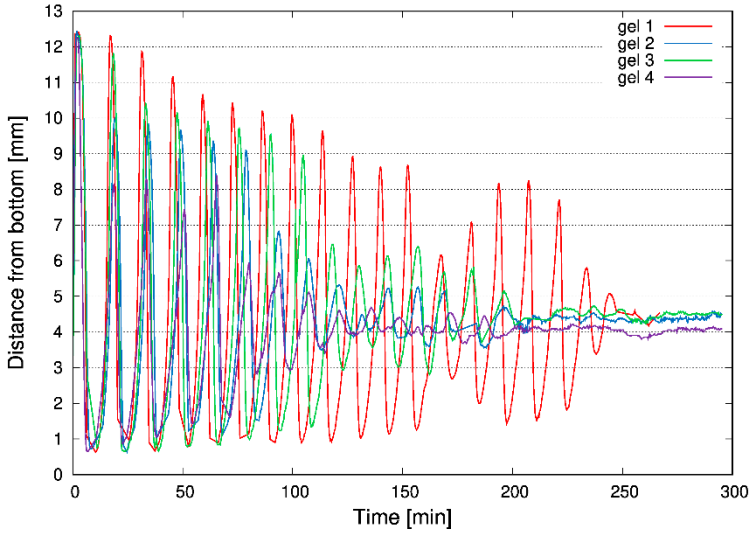

Figure 13. Vertical movements of case A gels in the PAANa solution.

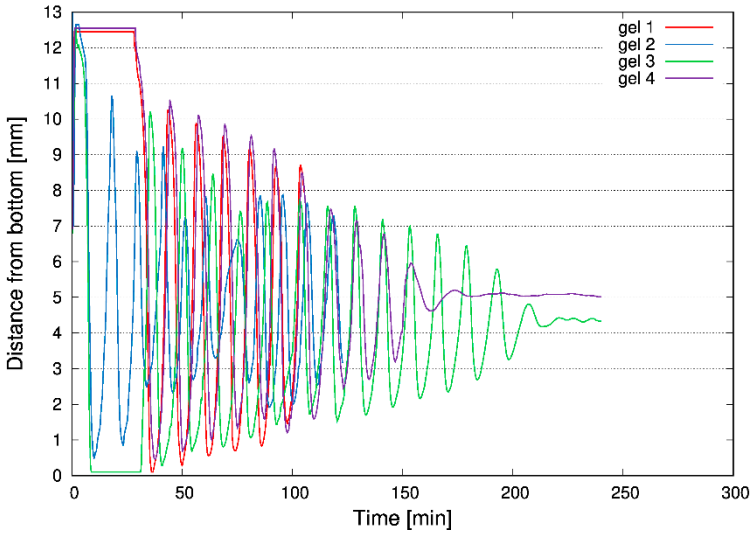

Figure 14. Case B in the PAANa solution.

Figure 15 showed the results for case C. At the start, gel 1 was positioned at ~5 mm from the bottom of the cavity in a state of shrinkage. It then started to move downward until it reached a position at 2 mm above the base of the cavity. At this level, the gel was affected by the lower temperature of the cooling source, and it started to swell; a quantity of surrounding fluid entered the gel's structure, and its diameter slowly increased. The gel's density became lower than that of the surrounding PAANa solution, and it started to gradually move upward until it reached a position at 3.5 mm above the base of the cavity. In this position, the gel started to shrink again because of the higher temperature of the surrounding fluid. A specific amount of aqueous polymer solution was squeezed out of the gel's structure, and its density became higher than that of the solution. Consequently, the gel moved downward again until it reached a position 3 mm above the base of the cavity. Over time, only very small fluctuations in position were observed, and the gel became stagnant at 2.8 mm above the base of the cavity. In this case, the up-down movement was only seen during approximately the first 20 min. Similar patterns of small initial amplitudes and short continuations of up-down movements were observed for case D, as shown in Figure 16. There is a difference in the oscillation modes of the gels in cases B and C, which could not be clarified in this study. However, the up-down movement continued until the gels and their surrounding fluids reached a state of equilibrium, at which point

the gravitational force and buoyancy force exerted on the gels canceled each other out. This occurred more quickly for the smaller gels and is qualitatively reasonable because the smaller gels could achieve relatively quicker heat and mass transfer with their surrounding fluids.

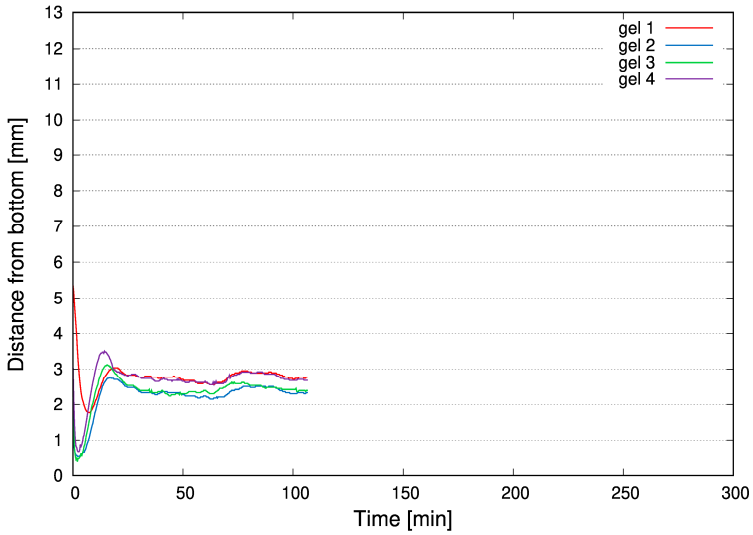

Figure 15. Case C in the PAANa solution.

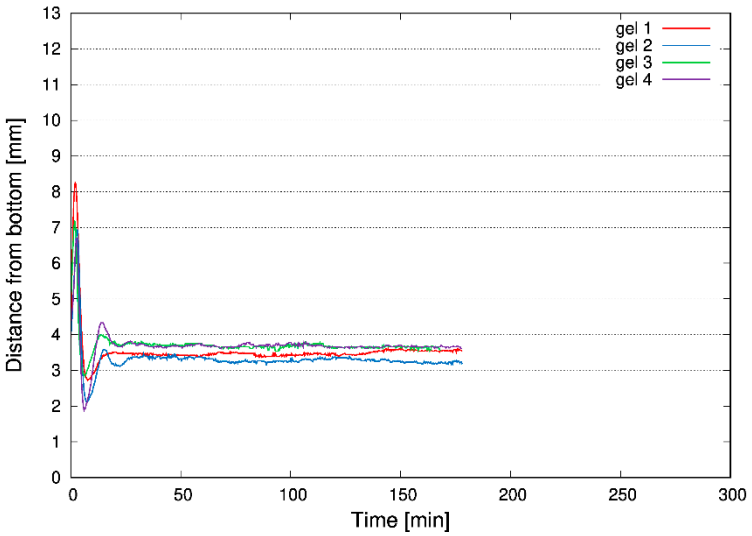

Figure 16. Case D in the PAANa solution.

4. Conclusions

When producing spherical gel particles, the diameter of the gel droplets can be controlled by adjusting the continuous-phase flow rate and the kinematic viscosity. Both shrinking and swelling of the gels occurred after polymerization because of changes in the ambient temperature of the polymeric solution, which resulted in negative thermal expansion. The gel particles required a certain length of time to thoroughly respond to the temperature changes of the PAANa polymeric solution in both swollen and shrunken states. In fact, more than 10 min were required for the gels to swell and shrink to their steady-state particle size. This phenomenon affected the floating behavior of the gel particles in the polymeric aqueous solutions. When the temperature of the polymeric solution was 40 °C, the density of the gel particles was greater than that of the surrounding polymeric solution; moreover, the gel particles tended to settle because the acting gravitational force was greater than the buoyancy force. However, when the temperature was adjusted to 10 °C, the gel particles' densities were lower than that of the

aqueous solution. Furthermore, because buoyancy force exceeded gravitational force, the particles tended to float. The gels with larger diameters tended to have longer vertical periodic movements and required more time to reach their equilibrium state compared with gels with smaller diameter.

Author Contributions: Conceptualization, M.H.; methodology, M.H.; validation, R.R.S. and M.H.; investigation, R.R.S., K.N., and Y.N.; writing, R.R.S., K.N., and M.H.; supervision, M.H. and Y.T. All authors have read and agreed to the published version of the manuscript.

Funding: This research was funded by JSPS KAKENHI, grant number JP17K06191, and the Indonesia Endowment Fund for Education (LPDP) in providing funding via a BUDI-LN Scholarship Scheme.

Conflicts of Interest: The authors declare no conflict of interest.

References

1. Matanovic, M.R.; Kristl, J.; Grabnar, P.A. Thermoresponsive polymers: Insight into decisive hydrogel characteristics, mechanisms of gelation, and promising biomedical applications. *Int. J. Pharm.* **2014**, *472*, 262–275. [CrossRef]
2. Ganorkar, C.R.; Liu, F.; Baudy, M.; Kim, S.W. Modulating insulin-release profile from pH/ thermosensitive polymeric beads through polymer molecular weight. *J. Control. Release* **1999**, *59*, 287–298. [CrossRef]
3. Hoffman, A.S. Intelligent polymers in medicine and bio-technology. *Artif. Organs* **1995**, *19*, 458–467. [CrossRef] [PubMed]
4. Ding, Z.; Fong, R.B.; Long, C.J.; Stayton, P.S.; Hoffman, A.S. Size-dependent control of the binding of biotinylated proteins to streptavidin using a polymer shield. *Nature* **2001**, *411*, 59–62. [CrossRef] [PubMed]
5. Jeong, B.; Kim, S.W.; Bae, Y.H. Thermosensitive sol-gel reversible hydrogels. *Advance Drug Delivery Rev.* **2002**, *54*, 37–51. [CrossRef]
6. Klouda, L. Thermoresponsive hydrogels in biomedical applications: A seven-year update. *Eur. J. Pharm. Biopharm.* **2015**, *97*, 338–349. [CrossRef]
7. Ward, M.A.; Georgiou, T.K. Thermoresponsive polymers for biomedical applications. *Polymer* **2011**, *3*, 1215–1242. [CrossRef]
8. Boustta, M.; Colombo, P.E.; Lenglet, S.; Poujol, S.; Vert, M. Versatile UCST-based thermoresponsive hydrogels for loco-regional sustained drug delivery. *J. Control. Release* **2014**, *174*, 1–6. [CrossRef]
9. Iizawa, T.; Taketa, H.; Maruta, M.; Ishido, T.; Gotoh, T.; Sakohara, S. Synthesis of porous poly (N-isopropylacrylamide) gels beads by sedimentation polymerization and their morphology. *J. Appl. Polym. Sci.* **2007**, *104*, 842–850. [CrossRef]
10. Sisworo, R.R.; Hasegawa, M.; Kawabata, N. Convective heat transfer inside a fluid-filled rectangular cavity. *Int. J. Appl. Eng. Res.* **2018**, *13*, 1789–1797.
11. Wang, H.D.; Chu, L.Y.; Yu, X.Q.; Xie, R.; Yang, M.; Xu, D.; Zhang, J.; Hu, L. Thermosensitive affinity behavior of poly(N-isopropylacrylamide) hydrogels with β-cyclodextrin moieties. *Ind. Eng. Chem. Res.* **2007**, *46*, 1511–1518. [CrossRef]
12. Zhang, N.; Zheng, S.; Pan, Z.; Liu, Z. Phase transition effects on mechanical properties of NIPA hydrogel. *Polymers* **2018**, *10*, 358. [CrossRef] [PubMed]
13. Hasegawa, M.; Kamikido, T.; Kawabata, N. Behavior of thermo-sensitive gel in polymer solution. *Int. Commun. Heat Mass Transf.* **2016**, *76*, 55–58. [CrossRef]
14. Oh, K.S.; Oh, J.S.; Choi, H.S.; Bae, C.Y. Effect of cross-linking density on swelling behavior of NIPA gel particles. *Macromolecules* **1998**, *31*, 7328–7335. [CrossRef]
15. Li, Y.; Tanaka, T. Study of the universality class of the gel network system. *Journal of Chemical Physics.* **1989**, *90*, 5161. [CrossRef]
16. Zhang, X.Z.; Zhuo, R.X. Preparation of fast responsive, temperature-sensitive poly (*N*-isopropylacrylamide) hydrogel. *Macromol. Chem. Phys.* **1999**, *200*, 2602–2605. [CrossRef]
17. Zhang, X.Z.; Zhuo, R.X.; Yang, Y. Using mixed solvent to synthesize temperature sensitive poly(*N*-isopropylacrylamide) gel with rapid dynamics properties. *Biomaterials* **2002**, *23*, 1313–1318. [CrossRef]
18. Zhao, Q.; Sun, J.; Zhou, Q. Synthesis of macroporous poly (*N*-isopropylacrylamide) hydrogel with ultrarapid swelling-deswelling properties. *J. Appl. Polym. Sci.* **2007**, *104*, 4080–4087. [CrossRef]

19. Zhao, Q.; Sun, J.; Ling, Q.; Zhou, Q. Synthesis of macroporous thermosensitive hydrogels: A novel method of controlling pore size. *Langmuir* **2009**, *25*, 3249–3254. [CrossRef]
20. Bouquey, M.; Serra, C.; Berton, N.; Prat, L.; Hadziioannou, G. Microfluidic synthesis and assembly of reactive polymer beads to form new structured polymer materials. *Chem. Eng. J.* **2008**, *135*, S93–S98. [CrossRef]
21. Seo, M.; Nie, Z.; Xu, S.; Mok, M.; Lewis, P.C.; Graham, R.; Kumacheva, E. Continuous microfluidic reactors for polymer particles. *Langmuir* **2005**, *21*, 11614–11622. [CrossRef] [PubMed]
22. Nisisako, T.; Torii, T.; Higuchi, T. Novel microreactors for functional polymer beads. *Chem. Eng. J.* **2004**, *101*, 23–29. [CrossRef]
23. Zygan, Z.T.; Cabral, J.T.; Beers, K.L.; Amis, E.J. Microfluidic platform for the generation of organic-phase microreactors. *Langmuir* **2005**, *21*, 3629–3634.
24. Quevedo, E.; Steinbacher, J.; McQuade, D.T. Interfacial polymerization within a simplified microfluidic device: Capturing capsules. *J. Am. Chem. Soc.* **2005**, *127*, 10498–10499. [CrossRef] [PubMed]
25. Cramer, C.; Fischer, P.; Windhab, E.J. Drop formation in a co-flowing ambient fluid. *Chem. Eng. Sci.* **2004**, *59*, 3045–3058. [CrossRef]
26. Zhang, D.F.; Stone, H.A. Drop formation in viscous flows at a vertical capillary tube. *Phys. Fluids* **1997**, *9*, 2234–2242. [CrossRef]
27. Sandulache, M.; Paullier, P.; Bouzerar, R.; Yzet, T.; Baledent, O.; Salsac, A. Liquid injection in confined co-flow: Application to portal vein embolization by glue injection. *Phys. Fluids* **2012**, *24*, 081902. [CrossRef]
28. Lan, W.; Jing, S.; Guoa, X.; Li, S. Study on "interface—shrinkage—driven" breakup of droplets in co-flowing microfluidic devices. *Chem. Eng. Sci.* **2017**, *158*, 58–63. [CrossRef]
29. Wu, P.; Luo, Z.; Liu, Z.; Li, Z.; Chen, C.; Feng, L.; He, L. Drag-induced breakup mechanism for droplet generation in dripping within flow focusing microfluidics. *Chin. J. Chem. Eng.* **2015**, *23*, 7–14. [CrossRef]
30. Hong, Y.; Wang, F. Flow rate effect on droplet control in a co-flowing microfluidic device. *Microfluid. Nanofluid.* **2007**, *3*, 341–346. [CrossRef]
31. Wang, W.; Ngan, K.H.; Gong, J.; Angeli, P. Observations on single drop formation from a capillary tube at low flow rates. *Colloids Surf. A Physicochem. Eng. Asp.* **2009**, *334*, 197–202. [CrossRef]
32. Sugiura, S.; Nakajima, M.; Iwamoto, S.; Seki, M. Interfacial tension driven monodispersed droplet formation from microfabricated channel array. *Langmuir* **2001**, *17*, 5562–5566. [CrossRef]
33. Thorsen, T.; Roberts, R.W.; Arnold, F.H.; Quake, S.R. Dynamic pattern formation in a vesicle-generating microfluidic device. *Phys. Rev. Lett.* **2001**, *86*, 4163–4166. [CrossRef] [PubMed]
34. Scheele, G.F.; Meister, B.J. Drop formation at low velocities in liquid-liquid systems: Part I. Prediction of drop volume. *AIChE J.* **1968**, *14*, 9–15. [CrossRef]
35. Leong, J.; Lim, T.; Pogaku, R.; Chan, E. Size prediction of k-carrageenan droplets formed in co-flowing immiscible liquid. *Particuology* **2011**, *9*, 637–643. [CrossRef]
36. Umbanhowar, P.B.; Prasad, V.; Weitz, D.A. Monodispersed emulsion generation via drop break off in a coflowing stream. *Langmuir* **2000**, *16*, 347–351. [CrossRef]
37. Baroud, C.N.; Gallaire, F.; Dangla, R. Dynamics of microfluidic droplets. *Lab Chip* **2010**, *10*, 2032–2045. [CrossRef]
38. Chen, C.T.; Maa, J.R.; Yang, Y.; Chang, C. Drop formation from flat tip nozzles in liquid-liquid system. *Int. Commun. Heat Mass Transf.* **2001**, *28*, 681–692. [CrossRef]
39. Schneider, T.; Chapman, G.H.; Hafeli, U.O. Effects of chemical and physical parameters in the generation of microspheres by hydrodynamic flow focusing. *Colloid Surf. B Biointerfaces* **2011**, *87*, 361–368. [CrossRef]
40. Zhu, K.J.; Jiang, H.L.; Du, X.Y.; Wang, J.; Xu, W.X.; Liu, S.F. Preparation and characterization of hCG-loaded polylactide or poly(lactide-co-glycolide) microspheres using a modified water-in-oil-in-water (w/o/w) emulsion solvent evaporation technique. *J. Microencapsul.* **2001**, *18*, 247–260.
41. Gupta, A.; Matharoo, H.S.; Makkar, D.; Kumar, R. Droplet formation via squeezing mechanism in a microfluidic flow-focusing device. *Comput. Fluids* **2014**, *100*, 218–226. [CrossRef]
42. Christopher, G.F.; Anna, S.L. Microfluidic methods for generating continuous droplet streams. *J. Phys. D Appl. Phys.* **2007**, *40*, R319–R336. [CrossRef]

43. Nunes, J.K.; Tsai, S.S.H.; Wan, J.; Stone, H.A. Dripping and jetting in microfluidic multiphase flows applied to particle and fibre synthesis. *J. Phys. D Appl. Phys.* **2013**, *46*, 114002. [CrossRef] [PubMed]
44. Tan, Y.; Cristini, V.; Lee, A.P. Monodispersed microfluidic droplet generation by shear focusing microfluidic device. *Sens. Actuators B* **2006**, *114*, 350–356. [CrossRef]